GMR
The Original

SUSTAINABLE FABRICATION OF POLYMERIC NANOCOMPOSITE EMBEDDED WITH CUO NANOPARTICLES FROM TURBINARIA CONOIDES EXTRACT: A STRUCTURAL INSIGHT INTO WOUND HEALING ACTIVITY ON HACAT KERATINOCYTE CELLS

Gopika Mohanakumar[1], Bhurani Ritu[2], Sangevi Raam A[3], Anguchamy Veeruraj[4], Kaliyamoorthy Dass[5*]

[1]Saveetha Medical College & Hospital (SMCH), Saveetha Institute of Medical and Technical Sciences (SIMATS), Thandalam, Chennai, Tamil Nadu 602105, India.
[2]Postgraduate, Department of ENT, Saveetha Medical College and Hospital, Saveetha Institute of Medical And Technical Sciences (SIMATS), Thandalam, Chennai-602105, Tamil Nadu, India. Email: ritunagarajan@gmail.com; ORCID: https://orcid.org/0009-0009-9620-1088.
[3]Senior Resident, Department of Paediatrics, Saveetha Medical College and Hospital, Saveetha Institute of Medical And Technical Sciences (SIMATS), Thandalam, Chennai-602105, Tamil Nadu, India. Email: sangeviraam@gmail.com; ORCID: https://orcid.org/0009-0001-3219-0764.
[4]Saveetha Institute of Basic Medical Sciences (SIBMS), Saveetha Medical College and Hospital, Saveetha Institute of Medical and Technical Sciences (SIMATS), Saveetha University, Chennai, 602 105, Tamil Nadu, India. anguveeruraj@gmail.com, https://orcid.org/0000-0001-7456-6507
[5*]Natural Product and Vector Control Research Lab, Department of Pharmacology, Saveetha Medical College and Hospital, Saveetha Institute of Medical And Technical Sciences (SIMATS), Thandalam, Chennai-602105, Tamil Nadu, India. dass.smc@saveetha.com; kdassrsgc1987@gmail.com, https://orcid.org/0000-0002-4564-3275

ABSTRACT

This study explores the wound healing potential of starch/polyvinyl alcohol (PVA) electrospun nanoscaffolds embedded with biogenic copper oxide nanoparticles (CuO NPs) synthesized using Turbinaria conoides extract. The CuO NPs were characterized using UV-Visible spectroscopy, revealing a surface plasmon resonance (SPR) peak at 270–300 nm, confirming successful green synthesis. Fourier transform infrared (FTIR) spectroscopy identified functional groups involved in nanoparticle stabilization, while X-ray diffraction (XRD) confirmed a monoclinic crystalline structure. Scanning electron microscopy (SEM) showed uniform nanofibers with well-dispersed CuO NPs. Thermogravimetric analysis (TGA) demonstrated enhanced thermal stability in the nanocomposite scaffolds. The wound healing efficacy was evaluated using a scratch assay on HaCaT keratinocytes. At 100 µg/mL, starch/PVA/CuO-NPs nanoscaffolds achieved 98.55% wound closure, outperforming CuO NPs (86.55%) and algal extract (72.55%). Concentration-dependent enhancement in cell migration was observed, with nanoscaffolds exhibiting superior performance at all tested concentrations (6.25–100 µg/mL). These findings highlight the scaffold's potential as a bioactive wound dressing, leveraging the synergistic effects of biogenic CuO NPs and polymeric nanofibers for accelerated tissue regeneration.

KEYWORDS: Turbinaria conoides, Green synthesis, CuO nanoparticles, Starch/PVA/CuO-NPs nanoscaffolds, Wound healing.

INTRODUCTION

Wound healing is a fundamental biological process essential for restoring skin integrity and function after injury [1]. This complex, dynamic sequence involves tightly regulated phases hemostasis, inflammation, proliferation, and remodeling that collectively coordinate cellular and molecular events to achieve tissue repair [2]. However, chronic wounds and delayed healing remain significant clinical challenges, often caused by infections, oxidative stress, or underlying pathological conditions such as diabetes and vascular diseases [3]. These complications not only impair patient quality of life but also increase healthcare costs substantially [4]. Therefore, the development of advanced wound dressings that can promote accelerated healing, prevent infections, and provide a conducive microenvironment for tissue regeneration is critically important in modern biomedical research [5].

In recent years, nanotechnology has emerged as a promising approach for designing innovative wound healing materials [6]. Nanofibrous scaffolds fabricated by electrospinning mimic the extracellular matrix (ECM) architecture, offering a high surface-to-volume ratio, tunable porosity, and excellent mechanical properties conducive to cellular adhesion, proliferation, and differentiation [7]. Among the polymers used in electrospinning, starch and polyvinyl alcohol (PVA) have gained considerable attention due to their biodegradability, biocompatibility, and non-toxic nature [8]. Starch, a natural polysaccharide abundant in nature, supports cell proliferation and moisture retention, while PVA provides mechanical strength and flexibility [9]. The combination of these polymers into composite scaffolds facilitates the creation of ideal wound dressing materials that support natural healing processes while allowing controlled incorporation of therapeutic agents [10].

The incorporation of bioactive nanoparticles into polymeric nanofibers further enhances their wound healing efficacy by introducing additional functionalities such as antimicrobial, anti-inflammatory, and antioxidant activities [11]. Copper oxide nanoparticles (CuO NPs), in particular, have attracted significant interest due to their broad-spectrum antimicrobial properties and ability to promote angiogenesis and tissue regeneration [12]. CuO NPs generate reactive oxygen species (ROS) at controlled levels that can modulate inflammatory responses and stimulate fibroblast activity, essential for wound repair [13]. Importantly, green synthesis of CuO NPs using biological extracts is a sustainable and eco-friendly alternative to conventional chemical

methods [14]. Biological molecules such as polyphenols, flavonoids, and proteins act as natural reducing and stabilizing agents, minimizing toxic chemical usage and improving biocompatibility [15]. This biogenic synthesis not only offers an environmentally benign route but also endows the nanoparticles with enhanced bioactivity due to surface functionalization by phytochemicals [16].

Marine macroalgae have recently emerged as a valuable natural resource for the green synthesis of metal nanoparticles, owing to their rich phytochemical content and easy accessibility [17]. Brown algae, such as Turbinaria conoides, are especially notable for their abundant bioactive metabolites including fucoidans, polyphenols, carotenoids, and sulfated polysaccharides [18]. These compounds exhibit potent antioxidant, anti-inflammatory, and antimicrobial effects, making T. conoides an ideal candidate for synthesizing biologically active CuO NPs [19]. Furthermore, the coastal waters near Rameswaram, Tamil Nadu, India, provide a sustainable source of this brown macroalga, allowing regional utilization of marine biomass for biomedical applications [20]. Employing T. conoides extract in ultrasonic-assisted green synthesis ensures efficient extraction of active biomolecules, enhanced nanoparticle yield, and improved physicochemical properties suitable for incorporation into nanofibrous wound dressings [21].

Electrospinning has been widely recognized as a versatile technique for fabricating nanofibrous mats with controlled fiber diameters and morphology, which closely mimic native ECM [22]. Integrating biogenic CuO NPs within starch/PVA nanofibers can potentially synergize the beneficial properties of each component—biocompatibility, mechanical stability, and bioactivity—to produce multifunctional scaffolds [23]. These scaffolds not only provide physical support to the regenerating tissue but also impart antibacterial protection and stimulate cellular responses crucial for wound closure [24]. Previous studies have demonstrated that CuO NP-embedded electrospun fibers significantly enhance keratinocyte migration and proliferation, reduce microbial colonization, and modulate oxidative stress, thereby accelerating healing outcomes in both in vitro and in vivo models [25].

Despite these promising advances, the synthesis parameters, nanoparticle incorporation methods, and the biological efficacy of T. conoides-mediated CuO NP-loaded starch/PVA nanoscaffolds have not been extensively explored [26]. Understanding the interplay between polymer matrix, nanoparticle characteristics, and bioactivity is essential for optimizing scaffold design tailored for wound healing applications [27]. Moreover, employing ultrasonic-assisted extraction techniques can improve the yield and bioavailability of marine algal phytochemicals used in nanoparticle synthesis, thereby enhancing the therapeutic potential of the final composite scaffolds [27]. Comprehensive physicochemical characterization combined with biological evaluations such as scratch assays using keratinocyte cultures provides critical insight into the wound healing capabilities of these novel materials [28].

In this context, the present study aims to develop starch/PVA electrospun nanofibrous scaffolds embedded with biogenically synthesized CuO NPs derived from T. conoides extract via an ultrasonic-assisted method [29]. The objectives include detailed physicochemical characterization of the nanoparticles and scaffolds, investigation of their structural and thermal properties, and evaluation of wound healing potential using in vitro keratinocyte migration assays [30]. This interdisciplinary approach leverages the natural bioactivity of marine algae, the antimicrobial and regenerative properties of CuO NPs, and the advantageous scaffold architecture produced by electrospinning [31]. Such composite nanoscaffolds hold considerable promise as next-generation wound dressings, combining sustainability, efficacy, and biocompatibility for enhanced skin tissue regeneration [32].

2.MATERIALS AND METHODS

2.1. Chemicals and reagents

T. conoides, a brown macroalga native to the coastal waters near Rameswaram, Tamil Nadu, India, was selected as the biological source for the green synthesis of CuO NPs. Analytical grade copper (II) sulfate pentahydrate was employed as the precursor salt. PVA with an average molecular weight of ~115,000 g/mol and starch were utilized to fabricate nanofibrous scaffolds through electrospinning on a HOLMARC HO-NFES-040 apparatus. All solvents and reagents were procured from Merck and Sigma-Aldrich with analytical purity to ensure consistency and reliability. The synthesized nanoparticles and composite scaffolds underwent comprehensive physicochemical analyses and were subsequently tested for wound healing activity using validated bioassays.

2.2. Collection and preparation of algal biomass

Fresh T. conoides samples were hand-harvested from intertidal zones along the Rameswaram coastline. The collected algae were transported promptly to the laboratory in ice-cooled containers to preserve freshness. Surface contaminants, including epiphytes and sand particles, were removed by rinsing first with tap water, followed by several washes in distilled water to remove residual salts. Approximately 100 grams of clean algal fronds were cut into smaller pieces and air-dried under ambient room conditions for two weeks. Upon complete desiccation, the dried biomass was pulverized into a fine powder using a mechanical grinder and stored in airtight containers until further use in extraction and nanoparticle synthesis.

2.3. Ultrasonic-assisted extraction of phytochemicals

To isolate bioactive constituents, 2 g of the powdered algae was suspended in 50 mL Milli-Q water within a 100 mL borosilicate vessel. The mixture underwent ultrasonic extraction in a LABQUEST ultrasonic cleaner (Borosil, Serial No. 941032329018) at 60°C for 45 minutes, facilitating enhanced cell wall disruption and improved metabolite release. The resultant extract was filtered through Whatman No. 1 filter paper to remove insoluble debris. The clarified aqueous extract was stored at 10°C for subsequent experiments, with a portion freeze-dried to yield a stable powdered extract for use in nanoparticle synthesis [33, 34].

2.4. Green synthesis of CuO NPs

For the biogenic synthesis, 50 mL of 0.1 M copper sulfate solution was mixed with 10 mL of algal extract (equivalent to 10 mg dry biomass) at a 5:1 volumetric ratio. This mixture was stirred continuously at 650 rpm and heated to 60°C for 2 hours using a temperature-controlled magnetic stirrer. A noticeable color shift from deep blue to bluish-green confirmed the reduction of copper ions to CuO NPs by the phytochemicals. The resulting nanoparticles were centrifuged and washed thrice with double-distilled water to remove residual reactants. Finally, the purified CuO NPs were freeze-dried for 48 hours to obtain a powdered product [19].

2.5. Preparation of starch/PVA/CuO nanofibrous scaffolds

Nanofibrous scaffolds were fabricated by first preparing a 15% (w/w) aqueous PVA solution, achieved by dissolving the polymer in Milli-Q water under continuous stirring at 50°C. After complete dissolution, 100 mg of starch and the synthesized CuO NPs were added to the solution. This mixture was further stirred for 2.5 hours at the same temperature to ensure a uniform dispersion. The final homogeneous solution was loaded into a syringe fitted with a 0.84 mm stainless steel needle for electrospinning using a HOLMARC HO-NFES-040 system. Electrospinning was performed at ambient temperature with optimized settings: voltage of 11.5 kV, tip-to-collector distance of 12.3 cm, and flow rate of 0.4 mL/h. Nanofiber mats were collected continuously over 6 to 8 hours and stored in desiccators for further analysis [35-37].

2.6. Physicochemical characterization

2.6.1. UV–visible spectroscopy

UV–Vis spectra were recorded using a VIS SPEC V-730 spectrophotometer to evaluate the optical characteristics of the algal extract, CuO NPs, and their incorporation into scaffolds. Absorption measurements were taken across 200–800 nm with deionized water as the blank. Characteristic peaks observed between 270 and 300 nm indicated successful nanoparticle formation and scaffold integration [38].

2.6.2. Fourier Transform Infrared Spectroscopy (FTIR)

Functional group analysis and chemical interactions were investigated using a PerkinElmer Spectrum Two FTIR spectrometer in ATR mode. Spectra were recorded from 4000 to 400 cm^{-1}, averaging 64 scans at a resolution of 4 cm^{-1}. Peaks corresponding to hydroxyl, carbonyl, amide, and metal–oxygen vibrations confirmed the presence of bioactive molecules and the incorporation of nanoparticles [39].

2.6.3. X-ray Diffraction (XRD)

The crystalline phases of CuO NPs and their composites were identified using a Bruker D8 Advance X-ray diffractometer with CuKα radiation (λ = 1.5406 Å). Data were collected from 5° to 90° 2θ at 40 kV and 40 mA, with 0.029649° step increments. Distinct monoclinic CuO diffraction peaks verified crystallinity, while broadened peaks in composites indicated nanoparticle dispersion [40].

2.6.4. Scanning Electron Microscopy (SEM)

Surface morphology and fiber uniformity were analyzed with a JEOL JSM-IT800 SEM. Samples were sputter-coated with gold to minimize charging effects. Micrographs confirmed uniform fiber diameters and even CuO NP distribution, verifying the effectiveness of the electrospinning process [41].

2.6.5. Thermogravimetric Analysis (TGA)

Thermal stability was assessed on a PerkinElmer TGA 8000 instrument. Approximately 5 mg of each sample was heated from room temperature to 550°C at a rate of 15°C/min under nitrogen flow. Thermograms showed multi-step degradation patterns representing moisture evaporation, polymer decomposition, and improved thermal stability due to nanoparticle incorporation [42].

2.6.6. Particle size and zeta potential

The hydrodynamic diameter and surface charge of CuO NPs were measured using a Malvern Zetasizer Ultra. Dynamic Light Scattering (DLS) assessed particle size, while electrophoretic mobility measurements provided zeta potential values. Nanoparticles with zeta potentials beyond ±30 mV were considered colloidally stable for biological applications [43]. All characterization datasets are available on Mendeley Data (DOI: 10.17632/mmyv8mmkbx.2).

2.7. Wound healing (scratch) assay

The migratory capacity of HaCaT keratinocytes was evaluated using a scratch assay upon exposure to the test samples: algal extract, CuO NPs, and starch/PVA/CuO nanoscaffolds. Cells were seeded at 2×10^5 cells per well in 12-well plates with DMEM containing 10% fetal bovine serum and 1% penicillin-streptomycin, incubated at 37°C and 5% CO_2 until confluence. A sterile 200 µL pipette tip created a uniform scratch simulating a wound. After washing with PBS to remove debris, cells were treated with the test materials at concentrations of 6.25, 12.5, 25, 50, and 100 µg/mL in serum-free medium. Untreated wells served as controls. Wound closure was monitored microscopically at 0, 24, and 48 hours. ImageJ software quantified migration by calculating the percentage of wound closure for each treatment group [44].

2.8. Statistical analysis

Data from triplicate experiments were expressed as mean ± standard deviation and analyzed using SPSS v25.0 and GraphPad Prism v9.0. Statistical differences between groups were determined by one-way ANOVA with post-hoc tests (Tukey's or

Dunnett's) where appropriate. Significance was set at $p < 0.05$. Pearson correlation was applied to assess variable relationships. Normality was checked by the Shapiro–Wilk test; non-normal data were log-transformed before analysis. All results were interpreted with 95% confidence intervals to ensure statistical rigor [45].

3.RESULTS AND DISCUSSION

3.1. UV-visible spectroscopy

The UV–Visible absorption spectra of the aqueous extract from T. conoides, the biosynthesized CuO NPs, and the CuO-loaded starch/PVA nanoscaffolds were recorded using a JASCO V-730 spectrophotometer over the wavelength range of 200–800 nm (Figure 1). The crude seaweed extract displayed broad absorption bands at shorter wavelengths, typical of flavonoids and polyphenolic compounds known to absorb ultraviolet light owing to their conjugated π-electron systems.

The biosynthesized CuO NPs exhibited a prominent sharp absorption peak within the 270–300 nm region, attributed to surface plasmon resonance (SPR) effects. This SPR peak arises due to the collective oscillation of conduction electrons on the nanoparticle surface under light excitation. The distinct peak confirms the successful bioreduction of Cu^{2+} ions into CuO NPs by the seaweed's bioactive components.

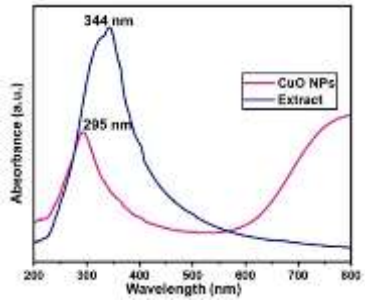

Figure 1. UV–Visible spectral profiles of algal extract and CuO NPs.

Incorporation of CuO NPs into starch/PVA nanofibers led to minor shifts and broadening in the absorption peaks compared to pure CuO NPs. These spectral modifications suggest molecular-level interactions, such as hydrogen bonding or van der Waals forces, between CuO NPs and polymer chains, supporting effective nanoparticle encapsulation and homogeneous distribution within the scaffold matrix. All spectral data were recorded in triplicate, with deionized water as the blank reference to exclude background interference [46].

3.2. FTIR spectroscopy

FTIR spectroscopy was used to identify functional groups involved in nanoparticle stabilization and their interaction with the polymeric matrix. Spectra for CuO NPs and CuO-loaded scaffolds were obtained using a PerkinElmer Spectrum Two FTIR spectrometer operating in ATR mode, scanning between 4000 and 400 cm^{-1} at a resolution of 4 cm^{-1} across 64 scans. The FTIR spectrum of the CuO NPs (Figure 2) showed characteristic Cu–O stretching bands at 590.53 cm^{-1} and 464.53 cm^{-1}, confirming the formation of copper oxide. Peaks at 801.66 cm^{-1} corresponded to C–H bending vibrations, while bands at 1015.22 cm^{-1} and 1065.56 cm^{-1} were associated with C–O stretching modes. The absorption at 1511.28 cm^{-1} was assigned to aromatic C=C or N–H bending vibrations. A broad O–H stretching band centered at 3166.88 cm^{-1} indicated phytochemical adsorption from the algae on the nanoparticle surface. For the CuO-loaded starch/PVA scaffold, the FTIR spectra revealed new and shifted peaks confirming nanoparticle integration. The Cu–O band shifted slightly to 603.51 cm^{-1}. Additional notable bands at 843.42 cm^{-1} (C–H bending), 913.12 cm^{-1} (C–O–C stretching), and 1089.99 cm^{-1} (C–O stretching) reflected polysaccharide and ether groups. Vibrations at 1425.37 cm^{-1} and 2923.53 cm^{-1} were attributed to C–H groups, while peaks at 1711.84 cm^{-1} and 1732.70 cm^{-1} indicated ester and carbonyl groups from PVA. The broad O–H stretch at 3296.86 cm^{-1} suggested hydrogen bonding, which supports the formation of a stable polymer-nanoparticle interaction network [47

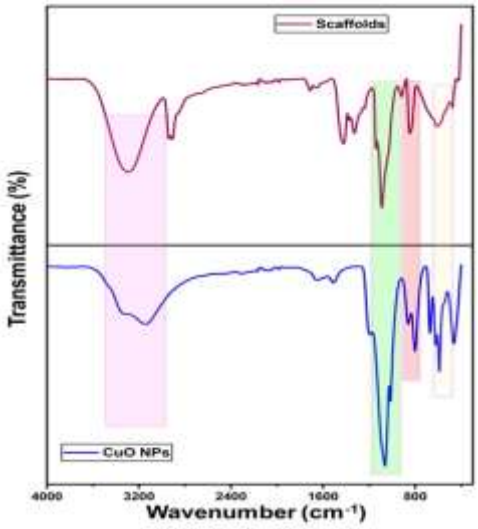

Figure 2. FTIR spectra of CuO NPs and their incorporation into nanoscaffolds.

3.3. XRD analysis

XRD analysis was conducted to examine the crystallinity and nanoparticle incorporation within the nanoscaffolds. Measurements were performed using a Bruker D8 Advance diffractometer with CuKα radiation (λ = 1.5406 Å) at 40 kV and 40 mA, scanning 2θ angles from 5° to 90° at a step size of 0.029649° (Figure 3). The diffraction pattern of the CuO NPs exhibited sharp, distinct peaks characteristic of a monoclinic crystal structure, consistent with JCPDS card No. 48-1548. Prominent reflections appeared at 15.666°, 16.451°, 17.368°, 20.181°, 24.173°, 26.071°, 28.492°, 31.764°, 32.614°, 35.035°, 38.242°, and 47.468°. The highest intensity peak at 26.071° corresponded to a d-spacing of 3.41519 Å with a narrow full width at half maximum (FWHM) of 0.100°, indicating small crystallite size.

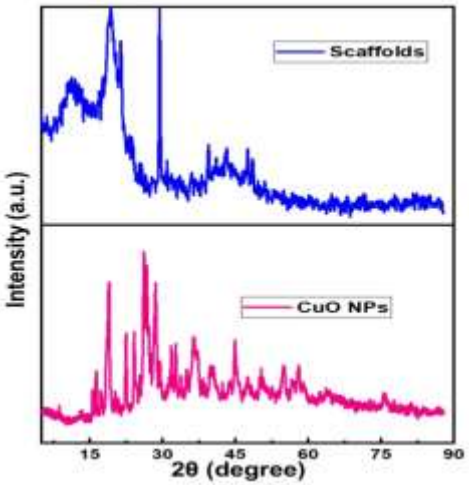

Figure 3. XRD patterns of synthesized CuO NPs and CuO-loaded scaffolds.

The XRD profile of CuO-loaded starch/PVA nanoscaffolds showed semi-crystalline nature with peaks at 11.332°, 19.284°, 21.272°, 23.481°, 29.372°, 30.771°, 35.778°, 39.533°, and 47.559°. The prominent reflection at 29.372° (d = 3.03842 Å, FWHM = 0.170°) was attributed to the polymer matrix. Peaks at 30.771° and 35.778° corresponded to CuO, confirming retention of nanoparticles in the scaffold. Peak broadening and slight shifts indicated a decrease in crystallite size and lattice strain due to polymer–nanoparticle interaction. The monoclinic CuO phase remained intact after embedding [49].

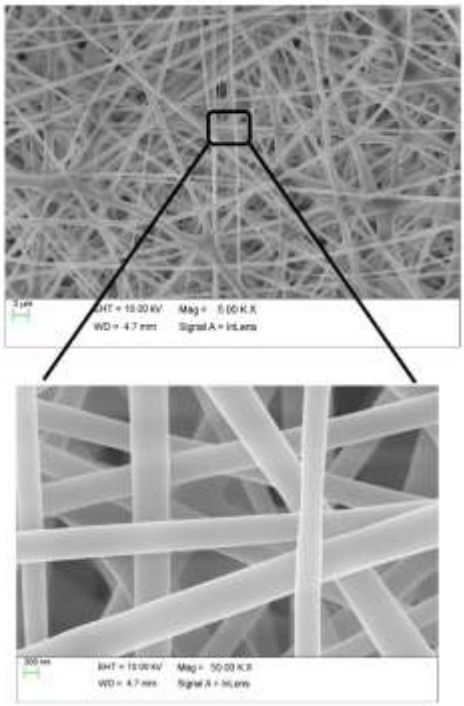

Figure4. SEM analysis of starch/PVA/CuO-NPs nanoscaffolds

3.4. SEM analysis

The surface morphology of CuO NPs and nanoscaffolds was examined using a JEOL JSM-IT800 NANO SEM. Samples were sputter-coated with gold to enhance conductivity prior to imaging. SEM images of the CuO NPs revealed mostly spherical shapes with occasional irregular morphologies, ranging in size from 60 to 90 nm. Some aggregation was observed, likely caused by the high surface energy of the particles driving attraction. SEM micrographs of CuO-starch/PVA scaffolds (Figure 4) showed uniform fibrous networks with fiber diameters between 90 and 110 nm. The fibers exhibited smooth surfaces with interconnected porosity be3neficial for drug delivery and tissue engineering, supporting cell attachment and nutrient exchange. The CuO NPs appeared well embedded within the nanofibers, evenly dispersed with minimal agglomeration, indicating successful incorporation via electrospinning. The consistent dispersion and uniform fiber morphology confirm optimized fabrication parameters for producing stable, functional nanocomposite scaffolds [50, 51].

3.5. TGA

Thermal stability of the CuO-loaded nanofibers was evaluated using a PerkinElmer TGA 8000 instrument. A 7.685 mg sample was heated from 30°C to 550°C at a rate of 15°C/min under nitrogen atmosphere (Figure 5). The thermogram showed two main degradation stages. The first degradation began at 326.78°C and peaked at 381.60°C with a mass loss of 34.960%, corresponding to decomposition of starch, PVA, and volatile organics. The second stage started at 438.61°C and peaked at 459.06°C with an additional 4.679% weight loss due to degradation of residual organic compounds and bioactive molecules bound to CuO. Compared with pure starch/PVA scaffolds, CuO-containing composites demonstrated delayed onset of thermal degradation, indicating enhanced thermal stability. This is attributed to the inorganic CuO NPs restricting polymer chain mobility and acting as a thermal barrier. Derivative thermogravimetry (DTG) curves further elucidated these transitions. The small residual mass at 550°C suggests nearly complete decomposition of organics, with CuO functioning as a thermal stabilizer within the composite matrix [50, 52, 53].

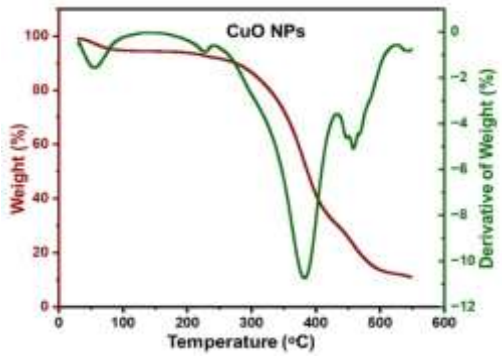

Figure 5. Thermal degradation behavior of CuO-incorporated nanoscaffolds.

3.6. Zeta potential and particle size analysis

DLS and zeta potential analyses were performed with a Malvern Zetasizer Ultra to determine particle size distribution and surface charge of the CuO NPs. The hydrodynamic diameter distribution revealed a dominant peak at 68.12 nm (Figure 6), consistent with SEM observations. The polydispersity index (PDI) was 0.5717, indicating moderate size heterogeneity.

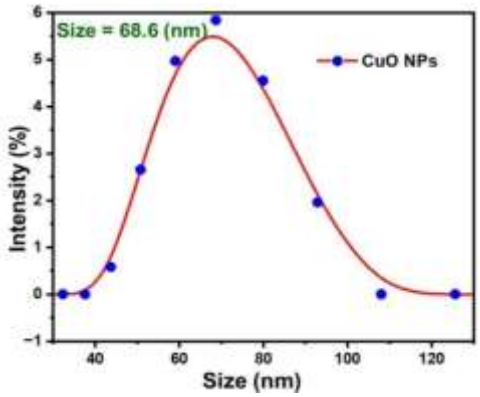

Figure6. DLS particles size analysis of CuO NPs

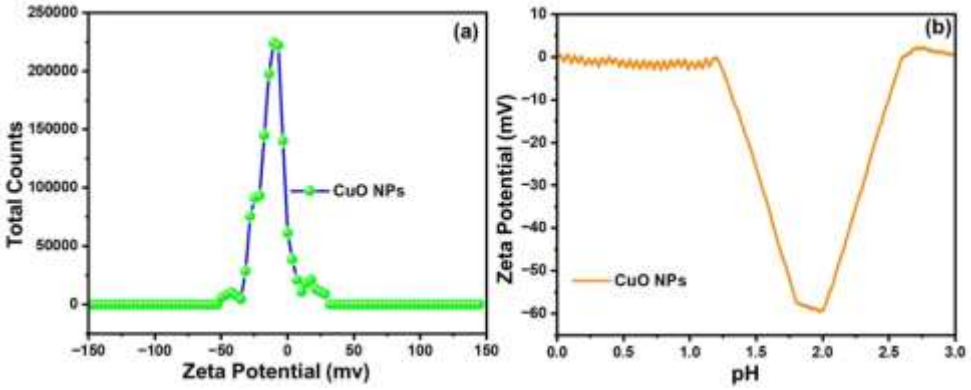

Figure7. Zeta-potential analysis of CuO NPs

Zeta potential measurements showed a main surface charge at −11.39 mV, along with minor peaks at −42.6 mV and −12.28 mV (Figure 7). The primary zeta potential value suggests limited electrostatic repulsion, which allows some aggregation over time. The presence of a more negatively charged fraction indicates partial colloidal stability. Overall, the zeta potential is below the ±30 mV threshold generally accepted as indicative of strong colloidal stability.

Conductivity was measured at 0.06892 mS/cm, and the count rate was 3.27 × 10^4 kcps, reflecting reasonable dispersion quality. For improved long-term stability in biomedical applications, further surface modification or use of stabilizers may be required. These findings offer important insights into the physicochemical stability and potential biomedical applicability of the CuO NPs [54, 55].

3.7. Wound healing (scratch) assay

The wound healing (scratch) assay results (Figure 8) demonstrated significant differences in the migratory behavior of HaCaT keratinocyte cells after 48 hours of treatment with algal extract, CuO NPs, and starch/PVA/CuO-NPs nanoscaffolds. At the lowest concentration (6.25 µg/mL), the algal extract exhibited a wound closure rate of 35.55%, while CuO NPs and nanoscaffolds showed higher closure rates of 43.55% and 50.55%, respectively. The control group, which received no treatment, had a baseline closure rate of 26%, indicating that all test samples enhanced cell migration compared to the untreated cells.

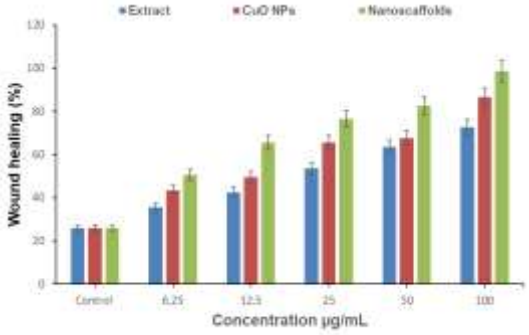

Figure 8. Wound healing activity analysis of algal extract, CuNPs and starch/PVA/CuONP

As the concentration increased to 12.5 µg/mL, the algal extract promoted a wound closure rate of 42.55%, whereas CuO NPs and nanoscaffolds further improved the healing process, achieving closure rates of 49.55% and 65.55%, respectively. This trend continued at higher concentrations, with the nanoscaffolds consistently outperforming both the algal extract and CuO NPs. At 25 µg/mL, the nanoscaffolds reached a remarkable 76.55% wound closure, compared to 53.55% for the algal extract and 65.55% for CuO NPs.

The most pronounced effects were observed at the highest concentration (100 µg/mL). Here, the algal extract achieved a 72.55% wound closure rate, while CuO NPs and nanoscaffolds demonstrated even greater efficacy, with closure rates of 86.55% and 98.55%, respectively. These results indicate that the nanoscaffolds were the most effective in accelerating wound healing, followed by CuO NPs, while the algal extract exhibited the least potent but still significant pro-migratory effects.

The wound healing assay revealed a concentration-dependent enhancement in cell migration for all test samples. The starch/PVA/CuO-NPs nanoscaffolds exhibited the highest wound closure rates across all concentrations, suggesting their superior potential in promoting keratinocyte migration and wound repair. CuO NPs also showed substantial activity, though slightly less than the nanoscaffolds, while the algal extract displayed moderate but consistent wound healing properties. These findings highlight the therapeutic potential of these materials in applications requiring accelerated tissue regeneration [56].

CONCLUSION

This study successfully demonstrated the wound healing potential of starch/PVA nanoscaffolds embedded with biogenic CuO NPs synthesized using T. conoides extract. Comprehensive characterization confirmed the formation of crystalline, spherical CuO NPs (60–90 nm) with phytochemical stabilization, as evidenced by UV-Vis, FTIR, and XRD analyses. SEM revealed uniform, porous nanofibers (90–110 nm) with well-dispersed nanoparticles, while TGA indicated enhanced thermal stability due to CuO incorporation. The scratch assay on HaCaT cells highlighted the scaffold's superior efficacy, achieving 98.55% wound closure at 100 µg/mL significantly higher than standalone CuO NPs (86.55%) or algal extract (72.55%). The concentration-dependent acceleration of keratinocyte migration underscores the scaffold's bioactive synergy, likely attributable to the combined effects of CuO's antimicrobial properties and the nanofibrous matrix's structural support for cell proliferation. These findings position the starch/PVA/CuO-NPs nanoscaffold as a promising, eco-friendly wound dressing candidate, merging green nanotechnology with tissue engineering for enhanced regenerative outcomes. Further in vivo studies are warranted to validate its clinical applicability.

Ethical Declaration: Not applicable for this study.

Funding: Not available for this study.

Conflicts of Interest: The authors declare no conflicts of interest.

Data Availability Statement: The full dataset of physiochemical characterization associated with this work is published in Mendeley Data [Dataset] Green nanotechnology in biomaterials: characterization of starch-based scaffolds with Turbinaria conoides-synthesized copper oxide nanocomposites (DOI: 10.17632/mmyv8mmkbx.1). **Disclosure:** The material characterization data and figures (e.g., UV, SEM, FTIR, XRD, TGA, Zeta Potential and particle sizer) presented here were generated from a common dataset and are being reused across multiple related studies on nanomaterials. All biological analyses and conclusions are original to each manuscript.

REFERENCES

1. Pei J, Palanisamy CP, Jayaraman S, Natarajan PM, Umapathy VR, Roy JR, Panagal M, Jayaraman S. Curcumin-loaded polymeric nanomaterials as a novel therapeutic strategy for Alzheimer's disease: A comprehensive review. Ageing Research Reviews. 2024; 99: 102393.
2. Pei J, Palanisamy CP, Jayaraman S, Natarajan PM, Umapathy VR, Roy JR, Thalamati D, Ahalliya RM, Kanniappan GV, Mironescu M. A comprehensive review on starch-based Sustainable Edible Films Loaded with Bioactive Components for Food Packaging. International Journal of Biological macromolecules. 2024; 274 (Part-1): 133332.
3. Palanisamy CP, poompradub S, Sansanaphongpricha K, Subramani K, Sonsudin F. Increased expression levels of PDGF and VEGF magnify the wound healing potential facilitated by biogenic synthesis of silver nanoparticles. Nano-Structures & Nano-Objects. 2024; 39: 101236.
4. Pei J, Palanisamy CP, Jayaraman S, Natarajan PM, Umapathy VR, Roy JR, Thalamati D, Ahalliya RM, Kanniappan GV, Mironescu M. Proteomics Profiling of Extracellular Vesicle for Identification of Potential Biomarkers in Alzheimer's Disease: A Comprehensive Review. Ageing Research Reviews. 2024; 99: 102359.
5. Xi J, Wang T, Xian P, Liu X, Du M, Yang H, Palanisamy CP, Lin W, Long Q. Proteomic insights uncover enhanced neurotherapeutic potential in conditioned mesenchymal stem cell-derived extracellular vesicles. Extracellular Vesicle. 2024; 3: 100037.
6. Pei J, Natarajan PM, Umapathy VR, Swamikannu B, Sivaraman NM, Krishnasamy L, Palanisamy CP. Advancements in the synthesis and functionalization of zinc oxide-based nanomaterials for enhanced oral cancer therapy. Molecules. 2024; 29(11): 2706.

7. Gatasheh MK, Natarajan SR, Krishnamoorthy R, Alsulami TS, Rajagopal P, Palanisamy CP, Veeraraghavan VP, Jayaraman S. Molecular analysis to identify novel potential biomarkers as drug targets in colorectal cancer therapy: an integrated bioinformatics analysis. Molecular and Cellular Oncology. 2024; 11(1): 2326699.
8. Pei J, Yan Y, Jayaraman S, Rajagopal P, Natarajan PM, Umapathy VR, Gopathy S, Roy JR, Sadagopan CS, Thalamati D, Palanisamy CP, Mironescu M. A review on advancements in the application of starch-based nanomaterials in biomedicine: Precision drug delivery and cancer therapy. International Journal of Biological Macromolecules. 2024; 130746.
9. Pei JJ, Yan Y, Palanisamy CP, Jayaraman S, Natarajan PM, Umapathy VR, Gopathy S, Roy JR, Sadagopan JC, Thalamati D, Mironescu M. Materials-based drug delivery approaches: Recent advances and future perspectives. Green Processing and Synthesis. 2024; 13: 20230094.
10. Panneerselvam S, Viswaja K, Deepa E, Prathiba S, Rebecca FS, Nivedha RP, Rajagopal P, Veeraraghavan VP, Sridevi G, Palanisamy CP, Jayaraman S. Hypoglycemic Potential of Acalypha indica in Streptozotocin-Induced Type 2 Diabetic Rats. International Journal of Drug Delivery Technology. 2026; 16(26s):1038-1047.
11. Panneerselvam S, Viswaja K, Prathiba S, Rebecca FS, Nivedha RP, Rajagopal P, Fathima SJH, Veeraraghavan VP, Sridevi G, Palanisamy CP, Jayaraman S. Acalypha Indica Attenuates Insulin Resistance in STZ-Induced Type 2 Diabetic Male Rats: Mechanistic Study. International Journal of Drug Delivery Technology. 2026; 16(26s):1027-1037.
12. Manju NE, Natarajan A, Rebecca FS, Nivedha RP, Hemalatha R, Rajagopal P, Murali R, Veeraraghavan VP, Sridevi G, Palanisamy CP, Jayaraman S. Effect of Seendhil polyherbal formulation in attenuating type-2 diabetes in STZ-induced experimental rats. International Journal of Drug Delivery Technology. 2026; 16(26s):981-989.
13. Manju NE, Natarajan A, Rebecca FS, Nivedha RP, Hemalatha R, Rajagopal P, Murali R, Veeraraghavan VP, Sridevi G, Palanisamy CP, Jayaraman S. Molecular mechanism to identify the effects of Seendhil polyherbal preparation on IRS-1/AKT/GLUT4/NRF2-KEAP-1 mediated signaling in SFZ-induced type-2 diabetic adult male rats. International Journal of Drug Delivery Technology. 2026;16(26s):972-980.
14. Palanisamy CP, Poompradub S, Sansanaphongpricha K, Jayaraman S, Subramani K, Sonsudin F. Biosynthesis of silver nanoparticles (AgNPs) using ethanolic extract of Nigella sativa (L.) seeds promotes wound healing via PDGF and VEGF signalling pathways activation. Biocatalysis and Agricultural Biotechnology. 2023; 54: 102970.
15. Palanisamy CP, Pei JJ, Phaniendra A, Venkata AAN, Jayaraman S, Veeraragahavan VP, Sridevi G, Roy JR, Janaki CS, Thalamati D, Mironescu M, Luo Q, Chai Y, Long Q. New Strategy of Neurodegenerative Disease Treatment with Extracellular Vesicles (EVs) Derived from Mesenchymal Stem Cells (MSCs). Theranostics. 2023; 13(12):4138-4165.
16. Surendran N, Chandrasekaran G, Raju MV, Chandrasekaran MK, Ahalliya RM, Palanisamy CP, Kanniappan GV, Arcot R, Alharbi NS, Thiruvengadam M. Anti-inflammatory potential of ethanolic extract of Maranta arundinacea L.: Insights from COX-2 modulation and oxidative stress analysis. South African Journal of Botany. 2026; 195: 142-151.
17. Pei J, Senthilkumar MV, Hessini K, Subramaniyam S, Sivaramakrishnan R, Kanniappan GV, Jayaraman S, Palanisamy CP. Green fabrication of starch/PVA/CuO nanoscaffolds using marine macroalgae extract for enhanced anti-inflammatory activity. Sustainable Chemistry and Pharmacy. 2026; 51: 102397.
18. Balasubramanian V, Loganathan L, Muthuswamy K, Viswanathan TM, Raju MV, Chandrasekaran MK, Ahalliya RM, Poorasamy J, Palanisamy CP, Dominic S, Kanniappan GV. Anticancer therapeutic efficacy of PEGylated β-galactosidase from Aspergillus terreus in DMBA-induced breast cancer: Toxicological, molecular and histopathological evaluation in Wistar rats. International Journal of Biological Macromolecules. 2026; 360: 151856.
19. Jayaraman S, Eswaran A, Rajagopal P, Palanisamy CP, Veerakumar P, Veeraraghavan VP, Sirasanagandla SR. Neuroendocrine-associated epigenetic factors in cellular senescence: mechanisms and therapeutic implications. Biogerontology. 2026; 27(2): 64.
20. Ponnusamy B, Rajagopal P, Palanisamy CP, Veeraraghavan VP, Jayaraman S. Mechanistic Exploration of the anticancer activity of Justicia adhatoda Plant Leaf Ethanolic Extract against Colon Cancer Cells: An in silico and in vitro Approach. Asian Pacific Journal of Cancer Prevention. 2026; 27(3): 1069-1080.
21. Pei J, Saran VS, Sivaramakrishnan R, Kanniappan GV, Pandurangan V, Jayaraman S, Dhayalan VK, Mironescu M, Mironescu ID, Palanisamy CP. Ultrasonic-assisted, Sargassum ilicifolium (brown marine macroalgae)-mediated biogenic synthesis of CuO nanoparticles incorporated in starch/PVA electrospun nanoscaffolds: In vitro safety and antioxidant efficacy assessment. Bioorganic Chemistry. 2026; 173: 109679.
22. Raj MAPA, Subramaniyam S, Kanniappan GV, Jayaraman S, Palanisamy CP. Sustainable fabrication of starch/PVA/CuO electrospun nanoscaffolds from Turbinaria ornata (marine macroalgae) extract: Physicochemical characterization and antidiabetic evaluation. Kuwait Journal of Science. 2026; 53(2): 100545.
23. Pei J, Ganesh NS, Subramaniyam S, Sivaramakrishnan R, Kanniappan GV, Jayaraman S, Palanisamy CP. Sustainable fabrication of starch/PVA/CuO electrospun nanoscaffolds from Padina tetrastromatica (Brown macroalgae) extract: Physicochemical characterization and antidiabetic assessment. Sustainable Chemistry One World. 2026; 9: 100195.
24. Sakthiraj A, Sivaramakrishnan R, Subramaniyam S, Kanniappan GV, Pandurangan V, Jayaraman S, Dhayalan VK, Mironescu M, Mironescu ID, Palanisamy CP. Chemical Physics Impact. Starch/PVA electrospun nanoscaffolds loaded with ultrasonic-assisted green-synthesis of CuO nanoparticles from marine macroalgae (Gracilaria corticata) extract: Cytotoxicity and antioxidant analysis. 2026; 12: 101018.
25. Raju M, Chandrasekaran MK, Loganathan L, Ahalliya RM, Mironescu M, Mironescu ID, Palanisamy CP, Kanniappan GV. Lipid remodeling and ferroptosis in phosphatidylcholine-mediated tumor–stroma crosstalk. Frontiers in Molecular Biosciences. 2026; 13: 1742305.

26. Kunamalla R, Panagal M, Palanisamy CP. Biogenic synthesis and fabrication of starch/PVA/CuO electrospun nanoscaffolds from Sargassum ilicifolium (brown marine macroalgae) extract for anticancer activity on HT-29 and MCF-7 cancer cells. Biocatalysis and Agricultural Biotechnology. 2026; 72: 103923.
27. Pei J, Govindaraj H, Sivaramakrishnan R, Kanniappan GV, Pandurangan V, Dhayalan VK, Mironescu M, Mironescu ID, Jayaraman S, Palanisamy PC. Sustainable fabrication of biopolymer-based (starch/PVA) nanoscaffolds loaded with green-synthesized CuO nanoparticles from Sargassum wightii (marine macroalgae): Cytocompatibility and antioxidant activity. Biomaterials Advances. 2026; 182: 214660.
28. Pei J, Perumal NC, Meng P, Long Q, Palanisamy CP. Extracellular vesicle-based biosensors for Alzheimer's disease: A new frontier in precision diagnostics. Ageing Research Reviews. 2026; 113: 102904.
29. Shree P, Sivaramakrishnan R, Kanniappan GV, Pandurangan V, Jayaraman S, Dhayalan VK, Mironescu M, Mironescu ID, Palanisamy CP. Antioxidant and biocompatible CuO-starch/PVA nanoscaffolds via ultrasonic green synthesis using Turbinaria conoides (brown marine macroalgae). Medicine in Drug Discovery. 2025; 28: 100238.
30. Gong J, Lin J, Guan T, Pei J, Palanisamy CP, El-AtyFrom AMA. selenium tolerance to nanoplastic antagonism: Comprehensive characterization of L. casei SNUT1 and its extracellular vesicle–nanoselenium complex. Food Bioscience. 2025; 74: 107749.
31. Poochi SP, Sundarraj R, Raju MV, Chandrasekaran MK, Ahalliya RM, Palanisamy CP, Kanniappan GV, Kondapavuluri BK, Thiruvengadam M. Harnessing Nature: Computational and Experimental Insights Into Ipomoea obscura Metabolites for Bladder Cancer Therapy. Chemistry and Biodiversity. 2025; 0: e00909.
32. Dugganaboyana GK, Kannankumar MKG, Shivaramakrishna S, Raju MV, Chandrasekaran MK, Ahalliya RM, Panneerselvam N, Palanisamy CP, Kanniappan GV. Phytochemical insights, antioxidant activity and therapeutic potential of Cassia senna against prostate cancer in Wistar albino rats. Discover Applied Sciences. 2025; 7:1206.
33. Natarajan SR, Krishnamoorthy R, Alshuniaber MA, Gatasheh MK, Rajagopal P, Veeraraghavan VP, Palanisamy CP, Jayaraman S. KDM1A Facilitates Oncogenic Potential in Colorectal Cancer Progression Through the Activation of AXIN/GSK3β/β-Catenin Signaling Pathways: Evidence From Integrated Transcriptomics and In Vitro Studies. The Journal of Gene Medicine. 2025; 27(11): e70053.
34. Guan T, Gong J, Lin J, Palanisamy CP, Jinjin Pei J, El-Aty AMA. Machine learning-driven multimodal optimization of selenium biotransformation and flavor profiling in fermented apple–Yacon functional beverages. Innovative Food Science & Emerging Technologies. 2025; 105: 104198.
35. Natarajan SR, Krishnamoorthy R, Alshuniaber MA, Alsulami TS, Gatasheh MK, Rajagopal P, Palanisamy CP, Govindan R, Veeraraghavan VP, Jayaraman S. ABCE1 facilitates tumour progression via aerobic glycolysis and inhibits cell death in human colorectal cancer cells through the p53 signalling pathway. Scientific Reports. 2025; 15: 24674.
36. Huang Y, Guo H, Liu Y, Jin W, Palanisamy CP, Pei J, Oz F, El-Aty AMA. Effects of Natural Polysaccharides on the Gut Microbiota Related to Human Metabolic Health. Molecular Nutrition & Food Research. 2025; 69:e202400792.
37. Poornima K, Meenakshi K.C, Manikandan V.R, Shankari G, Prabhu D, Rathi M.A, Palanisamy CP, Balaji R, Gopalakrishnan V.K. Exploring the anticancer potential of Jerantinine A from Tabernaemontana coronaria against prostate, breast, and ovarian cancers: A computational approach. Journal of Complementary and Integrative Medicine, 2025 22(2): 363–372.
38. Palanisamy CP, Poompradub S, Sansanaphongpricha K, Jayaraman S, Subramani K. Faridah Sonsudin gGreen synthesis of Nigella sativa-mediated silver nanoparticles for enhanced antibacterial activity and wound healing: Mechanistic insights and biomedical applications. Environmental Nanotechnology, Monitoring & Management. 2025; 24: 101085.
39. Surendran N, Raju MV, Chandrasekaran MK, Ahalliya RM, Palanisamy CP, Chandrasekaran G, Kanniappan GV. Physicochemical characterization of starch from Maranta arundinacea L.(arrowroot) rhizomes and its inhibition of COX-2: In vivo validation. Bioactive Carbohydrates and Dietary Fibre. 2025; 33: 100465.
40. Kannappan P, Chandrasekaran MK, Raju MV, Gopalakrishnan S, Dhamodharan P, Ahalliya RM, Palanisamy CP, Raju B, Kanniappan GV. Exploring the anticancer potential of Jerantinine A from Tabernaemontana coronaria against prostate, breast, and ovarian cancers: a computational approach. Journal of Complementary and Integrative Medicine. 2025; 22(02): 363-372.
41. Pei J, Kumarasamy RV, Jayaraman S, Kanniappan GV, Long Q, Palanisamy CP. Quercetin-functionalized nanomaterials: Innovative therapeutic avenues for Alzheimer's disease management. Ageing Research Reviews. 2025; 104: 102665.
42. Jayaraman S, Prasad M, Natarajan SR, Krishnamoorthy R, Alshuniaber MA, Gatasheh MK, Veeraraghavan VP, Rajagopal P, Palanisamy CP. Molecular mechanisms underlying the effects of beta-sitosterol on TGF-β1/Nrf2/SIRT1/p53-mediated signaling in the kidney of a high-fat diet and sucrose-induced type-2 diabetic rat. Chemico-Biological Interactions. 2025; 411: 111443.
43. Huang Y, Guo H, Liu Y, Jin W, Palanisamy CP, Pei J, Oz F, El-Aty AMA. Effects of Natural Polysaccharides on the Gut Microbiota Related to Human Metabolic Health. Molecular Nutrition & Food Research. 2025; e202400792.
44. Prabhakaran P, Palanisamy CP, Shanmugam A, Damodharan P, Swaminathan H, Devaraj D, Ahalliya RM, Kanniappan GV. Isolation, structural characterization, and molecular docking studies on the bioactive compound from n-Hexane extract of Emilia sonchifolia (L.) DC against the pancreatic cancer target Aurora 2 Kinase. Journal of Complementary and Integrative Medicine. 2024; 22(1): 0290.
45. Jiang H, Kumarasamy RV, Pei J, Raju K, Kanniappan GV, Palanisamy CP. Integrating engineered nanomaterials with extracellular vesicles: Advancing targeted drug delivery and biomedical applications. Frontiers in Nanotechnology. 2024; 6: 1513683.

46. Guo H, Liu Y, Wan T, Song D, Palanisamy CP, Geng J, Pei J, Özmen S, El-Aty AMA. Toward personalized cancer management: Role of precision nutrition–diet interventions. Journal of Functional Foods. 2024; 123: 106584.
47. Natarajan SR, Krishnamoorthy R, Alshuniaber MA, Al-Anazi KM, Farah MA, Rajagopal P, Palanisamy CP, Veeraraghavan VP, Jayaraman S. Identification of FOXM1 as a novel protein biomarker and therapeutic target for colorectal cancer progression: Evidence from immune infiltration and bioinformatic analyses. International Journal of Biological Macromolecules. 282 (Part 4): 137201.
48. Rajendran MS, Jayaraman S, Khan JM, Jasmine S, Prabhakaran RK, Raju MV, Chandrasekaran MK, Ahalliya RM, Kannappan P, Palanisamy CP, Kanniappan GV. Investigating the colon toxicity and carcinogenic role of monosodium glutamate compared with Dimethylhydrazine in male Wistar rats: Exploring the link to childhood colon cancer risk. Journal of King Saud University - Science. 2024; 36(11): 103507.
49. Kumarasamy RV, Natarajan PM, Umapathy VR, Roy JR, Rab SO, Saeed M, Panagal M, Mironescu M, Srinivasan GP, Palanisamy CP. Clinical Applications and Therapeutic Potentials of Advanced Nanoparticles: A Comprehensive Review on Completed Human Clinical Trials. Frontiers in Nanotechnology. 2024; 6:1479993.
50. Jin W, Pei JJ, Roy JR, Jayaraman S, Ahalliya RM, Kanniappan GV, Mironescu M, Palanisamy CP. Comprehensive review on single-cell RNA sequencing: A new frontier in Alzheimer's disease research. Ageing Research Reviews. 2024; 274: 102454.
51. Yang F, Bai X, Dai X, Li Y. The biological processes during wound healing, Regenerative medicine. 2021; 16(4): 373-390.
52. Iliaens J, Onsea J, Hoekstra H, Nijs S, Peetermans WE, Metsemakers WJ. Fracture-related infection in long bone fractures: a comprehensive analysis of the economic impact and influence on quality of life. Injury. 2021; 52(11): 3344-3349.